Anisotropic features in XMCD spectra

Shin-ichi Nagamatsu* and Takashi Fujikawa

Graduate School for Science, Chiba University, Yayoi-cho 1-33, Inage-Ku, Chiba, 263-8522 Japan. E-mail: nagamatu@scichem.s.chiba-u.ac.jp

We discuss the angular dependent *K*-edge X-ray Magnetic Circular Dichroism (XMCD) spectra based on the semi-relativistic full multiple scattering theory, where 2-spinor formalism is used to describe spin-orbit coupling. So far most of theoretical approaches have been limited to the simplest case where the circularly polarized X-ray propagation coincides with the direction of the magnetic field. Here we discuss more general cases, using the above theoretical approaches. We separately discuss atomic, single and full multiple scattering XMCD spectra; in particular anisotropic features of them are studied in detail.

Keywords: anisotropy in XMCD; **magnetic EXAFS.**

1. Introduction

XMCD has allowed us to measure element specific local magnetic properties. Some theoretical approaches have been developed and made remarkable achievements. Sum rules of the XMCD allow us to probe directly the orbital magnetization (Thole *et al.*, 1991; Igarashi & Hirai, 1994). Multiple scattering approach to the XMCD analyses are successful for the interpretation of Gd $L_{2,3}$-edge of rare earth and Fe *K*-edge XMCD (Ankudinov & Rehr, 1995; Brouder *et al.*, 1995). So far the XMCD studies have been restricted to the simplest case where the magnetization direction **M** and the circularly polarized X-ray propagation direction **k** are parallel to each other. However angular dependent XMCD spectra provide more information about spin quantization axis. The angular dependent XMCD spectra have been discussed by Carra *et al.* (Carra & Alterrelli, 1990) in the purely atomic picture. They derive a general formula to describe linear and circular dichroism in electric dipole and quadrupole excitation. Angular dependence for XMCD sum rules were discussed by van der Laan (van der Laan, 1998) in one-electron picture. Their theories take solid state effects into account by adjustment parameters. In contrast to these approaches the multiple scattering approaches can include solid state effect in transparent way. In Sec. 2, multiple scattering formula for the angular dependent *K*-edge XMCD is derived. The calculated XMCD for bcc Fe are compared with the observed one in Sec. 3.

2. Theory

2.1. Angular dependent XMCD

First we discuss the potential for an excited photoelectron. It is written in the sum of each atomic potential,

$$V(\mathbf{r}) = \sum_{\alpha} v^{\alpha}(\mathbf{r}_{\alpha})$$

where $v^{\alpha}(\mathbf{r}_{\alpha})$ is the atomic potential at site α, which is assumed to be spherical symmetric. As a relativistic correction we take only spin-orbit(SO) coupling into account in the 2-spinor formula, which yields

$$v^{\alpha} = v_c^{\alpha} + v_{ex}^{\alpha\pm} + \zeta^{\alpha}(r)\mathbf{S}\cdot\mathbf{L} \qquad (1)$$

where v_c^{α} is Coulomb potential, $v_{ex}^{\alpha\pm}$ is spin dependent exchange potential. The third term is the SO coupling potential, which is given by 2×2 matrix in the 2-spinor formula,

$$\zeta^{\alpha}(r)\mathbf{S}\cdot\mathbf{L} = \frac{\zeta^{\alpha}(r)}{2}\begin{pmatrix} L_z^{\alpha} & L_-^{\alpha} \\ L_+^{\alpha} & -L_z^{\alpha}\end{pmatrix}. \qquad (2)$$

Hereafter our attention is focused on light element systems, and the off-diagonal SO coupling term can be treated as weak perturbation δv^{α}, which contributes to spin-flip processes:

$$\begin{aligned} v^{\alpha} &= v_0^{\alpha} + \delta v^{\alpha}, \\ v_0^{\alpha\pm} &= v_c^{\alpha} + v_{ex}^{\alpha\pm} \pm \tfrac{\zeta^{\alpha}(r)}{2} L_z^{\alpha}, \\ \delta v^{\alpha} &= \tfrac{\zeta^{\alpha}(r)}{2}\begin{pmatrix} 0 & L_-^{\alpha} \\ L_+^{\alpha} & 0\end{pmatrix}. \end{aligned} \qquad (3)$$

The scattering Green's function at site α g_{α}^{0} for the scattering potential v_0^{α} is diagonalized as

$$g_{\alpha}^{0}(\varepsilon) = \begin{pmatrix} g_{\alpha}^{0}(\varepsilon)^{+} & 0 \\ 0 & g_{\alpha}^{0}(\varepsilon)^{-}\end{pmatrix} \qquad (4)$$

where $g_{\alpha}^{0\pm}$ denotes up and down spin Green's function which is written in terms of v_0^{α} and kinetic energy operator T_e

$$g_{\alpha}^{0}(\varepsilon)^{\pm} = (\varepsilon - T_e - v_0^{\alpha\pm} + i\eta)^{-1}. \qquad (5)$$

We can construct the full Green's function at site α including spin orbit coupling,

$$g_{\alpha} = g_{\alpha}^{0} + g_{\alpha}^{0}\delta v^{\alpha} g_{\alpha}^{0} + g_{\alpha}^{0}\delta v^{\alpha} g_{\alpha}^{0}\delta v^{\alpha} g_{\alpha}^{0} + \cdots. \qquad (6)$$

First we consider the simple geometrical setup; spin axis and the direction of the incident circularly polarized X-ray is parallel to each other. In this case electron-photon interaction operator Δ_{m_p} is given by $\Delta_{m_p} = rY_{1,m_p}(\hat{\mathbf{r}})$ neglecting unimportant constants. As usual we can utilize site T-matrix expansion of full Green's function g at an X-ray absorption atom A (Fujikawa, 1993)

$$g = g_A + \sum_{\alpha\neq A} g_A t_{\alpha} g_A + \sum_{\beta\neq\alpha\neq A} g_A t_{\alpha} g_0 t_{\beta} g_A + \cdots, \qquad (7)$$

where t_{α} is the site T-matrix at site α which is related to v^{α}, $t_{\alpha} = v^{\alpha} + v^{\alpha} g_0 t_{\alpha}$. g_0 is the free propagator and is different from g_{α}^{0} defined by eq. (5). Now we define $T(m_p, m_p')$ in terms of 1s core spinor function $|c\rangle$ and full Green's function g given by eq. (7),

$$T(m_p, m_p') = -\frac{1}{\pi}\mathrm{Im}\,\langle c|\,\Delta_{m_p}^{*} g \Delta_{m_p'}\,|c\rangle\,. \qquad (8)$$

Each of $T(m_p, m_p')$ is written as the sum of atomic term $T^{(0)}$, single scattering term $T^{(1)}$, and double scattering term $T^{(2)}$ and so on, $T = T^{(0)} + T^{(1)} + T^{(2)} + \cdots$. In the next step, let specify the geometrical setup considered in this work. The direction of magnetic field should be in the *z*-axis to use eqs. (1)-(4). The incident X-ray photons come into the target from positive z'-direction, which is in the *xz*-plane tilted with angle β (see Fig. 1).

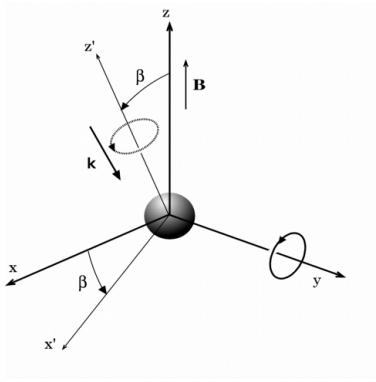

Figure 1
The geometrical setup in the XMCD experiment. The incident X-ray photons come into the target from positive z'-direction, which is in the xz-plane tilted with angle β.

The spherical harmonics Y_{1,m_p} written in $\hat{\mathbf{r}}'$ in the $x'y'z'$-coordinate system is related to those in $\hat{\mathbf{r}}$,

$$Y_{1,m_p}(\hat{\mathbf{r}}') = \sum_{\mu} Y_{1,\mu}(\hat{\mathbf{r}}) d^{(1)}_{\mu,m_p}(\beta). \tag{9}$$

Similar to eq. (8) we define the matrix elements $T'(m_p, m'_p)$ in the $x'y'z'$-coordinate system,

$$T'(m_p, m'_p) = -\frac{1}{\pi}\mathrm{Im}\,\langle c|\,\Delta'^{*}_{m_p} g \Delta'_{m'_p}\,|c\rangle\,, \tag{10}$$

where $\Delta'_{m_p} = rY_{1,m_p}(\hat{\mathbf{r}}')$. From eq. (9) we have a relation,

$$T'(m_p, m'_p) = \sum_{\mu,\mu'} d^{(1)}_{\mu,m_p}(\beta) d^{(1)}_{\mu',m'_p}(\beta) T(\mu,\mu'). \tag{11}$$

Substituting explicit formulas of $d^{(1)}$, we have an explicit formula for the X-ray circular dichroism for the general experimental arrangement shown in Fig. 1,

$$\begin{aligned} &T'(1,1) - T'(-1,-1) = \\ &\cos\beta\{T(1,1) - T(-1,-1)\} \\ &+\tfrac{\sin\beta}{\sqrt{2}}\{T(0,1) + T(1,0) + T(0,-1) + T(-1,0)\}. \end{aligned} \tag{12}$$

Of course, it is just $T(1,1) - T(-1,-1)$ when $\beta = 0°$. Typically we measure the XMCD under the condition, $\beta = 45°$.

2.2. Atomic XMCD

Because of the selection rule, only diagonal term $m_p = m'_p$ can contribute to the atomic term, the first term g_A in eq. (7). From eq. (12), angular dependent atomic XMCD is simply described by $\cos\beta\{T^{(0)}(1,1) - T^{(0)}(-1,-1)\}$. Carra *et al.* obtained the same result for the electric dipole transition (Carra & Alterrelli, 1990). The atomic X-ray absorption intensity $T^0(m_p, m_p)(m_p = \pm 1)$ is given by use of the perturbation expansion eq. (6) for g_A,

$$\begin{aligned} &T^{(0)}(m_p, m_p) = \\ &-\tfrac{1}{\pi}\mathrm{Im}\sum_{\sigma}\langle\sigma|\,\Delta^{*}_{m_p}(g^{0\sigma}_A + g^{0\sigma}_A \delta v^{\sigma\bar{\sigma}}_A g^{0\bar{\sigma}}_A \delta v^{\bar{\sigma}\sigma}_A g^{0\sigma}_A)\Delta_{m_p}\,|\sigma\rangle \end{aligned} \tag{13}$$

where σ and $\bar{\sigma} = -\sigma(= \pm 1/2)$ designate the spin state. As g^{0+}_A is different from g^{0-}_A because of different spin-polarization potential $v^{A\pm}_0$ in eq. (3), we can expect the nonzero contribution from the second term to $T^{(0)}(1,1) - T^{(0)}(-1,-1)$ which gives rise to the lowest order atomic XMCD.

2.3. Single and Multiple Scattering XMCD

By applying the site T-matrix expansion shown by eq. (7), we can write the single scattering X-ray absorption intensity $T^{(1)}(m_p, m'_p)$ up to the second order of ζ,

$$\begin{aligned} T^{(1)}(m_p, m'_p)_1 = &-\tfrac{1}{\pi}\mathrm{Im}\sum_{\sigma}\langle\sigma|\,\Delta^{*}_{m_p} g^{\sigma\sigma}_A t^{\sigma}_{\alpha} g^{\sigma\sigma}_A \Delta_{m'_p}\,|\sigma\rangle \\ &-\tfrac{1}{\pi}\mathrm{Im}\sum_{\sigma}\langle\sigma|\,\Delta^{*}_{m_p} g^{\sigma\bar{\sigma}}_A t^{\bar{\sigma}}_{\alpha} g^{\bar{\sigma}\sigma}_A \Delta_{m'_p}\,|\sigma\rangle \end{aligned} \tag{14}$$

where $|\sigma\rangle$ is the core state with spin σ, and no spin flip scattering take place at site α. Furthermore we should consider the spin flip scattering at site α,

$$\begin{aligned} T^{(1)}(m_p, m'_p)_2 = &-\tfrac{1}{\pi}\mathrm{Im}\sum_{\sigma}\langle\sigma|\,\Delta^{*}_{m_p} g^{\sigma\sigma}_A t^{\sigma\bar{\sigma}}_{\alpha} g^{\bar{\sigma}\sigma}_A \Delta_{m'_p}\,|\sigma\rangle \\ &-\tfrac{1}{\pi}\mathrm{Im}\sum_{\sigma}\langle\sigma|\,\Delta^{*}_{m_p} g^{\sigma\bar{\sigma}}_A t^{\bar{\sigma}\sigma}_{\alpha} g^{\sigma\sigma}_A \Delta_{m'_p}\,|\sigma\rangle \end{aligned} \tag{15}$$

The lowest order spin flip t-matrix $t^{\sigma\bar{\sigma}}_{\alpha}$ is given by, $t^{+-}_{\alpha} \approx \delta v^{+-}_{\alpha} = \zeta L_-/2, t^{-+}_{\alpha} \approx \delta v^{-+}_{\alpha} = \zeta L_+/2$. The lowest order spin flip Green's function g^{+-} at the X-ray absorption atom A is calculated based on perturbation theory with aid of eq. (6).

The multiple scatterings play an important role in the analyses of XANES spectra (Fujikawa, 1993). As far as we neglect the spin flip processes at the nearby atoms, we can renormalize the multiple scattering series, $T^{\infty} = T^{(0)} + T^{(1)} + T^{(2)} + \cdots$, which is crucial in the near edge XMCD analyses. For example $T^{\infty}(1,1) - T^{\infty}(-1,-1)$ is given by

$$\begin{aligned} &T^{\infty}(1,1) - T^{\infty}(-1,-1) = \\ &\tfrac{1}{2\pi^2}\mathrm{Im}\Big[\rho^{+-}(k)_c\rho^{-+}(k)_c\left\{G(1-X^{-})^{-1}\right\}^{A,A}_{10,10} \\ &-\rho^{-+}(k)_c\rho^{+-}(k)_c\left\{G(1-X^{+})^{-1}\right\}^{A,A}_{10,10}\Big], \end{aligned} \tag{16}$$

where $X = tG$ and $\rho^{\sigma\bar{\sigma}}(k)_c$ is spin flip radial dipole integral defined by

$$\rho^{\sigma\bar{\sigma}}(k)_c = \int dr R^{\sigma}_{1s}(r) r^3 \tilde{R}^{\sigma\bar{\sigma}}_1(kr),$$

where $\tilde{R}^{\sigma\bar{\sigma}}_1(kr)$ is the radial part of the spin flip scattering function with angular momentum $l = 1$.

Because we have $G(1-X^{-})^{-1} = G(1-X^{+})^{-1}$ for nonmagnetic systems, no XMCD is expected to be obtained if $\beta = 0$. If SO coupling is absent, the spin flip radial dipole integrals $\rho^{\sigma\bar{\sigma}}(k)_c$ vanish. As is well known, both of the spin polarization and the SO interaction are essential for the XMCD interpretation.

3. Results and discussion

Fig. 2 shows the atomic XMCD discussed in subsection 2.1, and the single scattering XMCD (magnetic EXAFS) spectrum discussed in subsection 2.2 for Fe K-edge compared with the experimental result by Schütz *et al.* (Schütz & Ahlers, 1997). The atomic XMCD is smooth as a function of energy, whereas the scattering effects give rise to rapid oscillation. In the low energy region, atomic XMCD cannot be neglected whereas it decays rapidly; in the EXAFS region, it is about 2 % of the magnetic EXAFS. The calculated spectrum including the single scattering term gives main features of experimental one, though for the detailed analysis we should include multiple scattering.

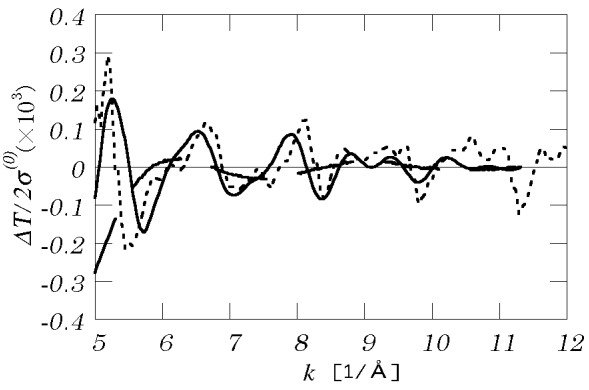

Figure 2
The calculated normarized XMCD spectra $\Delta T^{(0)} = T^{(0)}(1,1) - T^{(0)}(-1,-1)$ (atomic) and $\Delta T = \Delta T^{(0)} + \Delta T^{(1)}$(atomic + single scattering) of Fe K-edge in bcc Fe. $\Delta T^{(0)} \times 20$ (long dashed line) and ΔT (solid line) are compared with the experimental result (Schütz & Ahlers, 1997) shown by dotted line. $\sigma^{(0)}$ means $2\sigma^{(0)} = T^{(0)}(1,1) + T^{(0)}(-1,-1)$ (atomic absorption). For the single scattering calculation we use a cluster with 59 atoms.

We study the angular dependence of magnetic EXAFS. Fig. 3 shows the single scattering X-ray absorption intensity $\Delta T^{(1)} = T^{(1)}(1,1) - T^{(1)}(-1,-1)$, and $\delta T^{(1)} = T^{(1)}(1,0) + T^{(1)}(0,1) + T^{(1)}(-1,0) + T^{(1)}(0,-1)$ in eq. (12). The scatterers $\alpha = (a,a,a)$ and $\alpha' = (a,a,-a)$ give different interesting oscillations; $\Delta T^{(1)}$ is quite similar for both scatterers, whereas $\delta T^{(1)}$ for the scatterer α is $-\delta T^{(1)}$ for the scatterer α'. The latter finding is explained by use of the symmetry of $G_{L,L'}(k\mathbf{R})$ where L means angular momentum $L = (l,m)$. This example demonstrates that the latter contribution $\delta T^{(1)}$ usually have negligibly small contribution for highly symmetric systems because $\delta T^{(1)}$ is fully cancelled out.

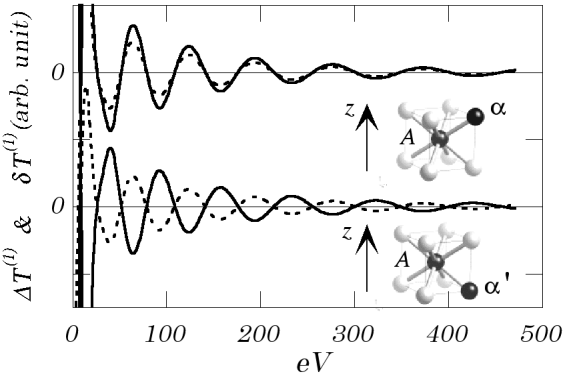

Figure 3
Comparison of the single scattering Fe K-edge XMCD from the different scatterer α and α'. The solid lines show $\delta T^{(1)} = T^{(1)}(1,0) + T^{(1)}(0,1) + T^{(1)}(-1,0) + T^{(1)}(0,-1)$, and the dashed lines $\Delta T^{(1)} = T^{(1)}(1,1) - T^{(1)}(-1,-1)$ (see eq. (12)). The site A denotes X-ray absorption atom. The energy zero is the same as that in Fig. 2.

Fig. 4 shows the calculated Fe K-edge XMCD spectrum compared with the experimental one ($\beta = 45^\circ$) in the near edge region. As discussed in the subsection 2.3, full multiple scatterings play an essential role. The agreement with the experimental is satisfactory in the energy range 7-25 eV. The peak at 30 eV is not reproduced in our calculation; which requires further studies. The second part in eq. (12) proportional to $\sin\beta$ is found to be negligibly small.

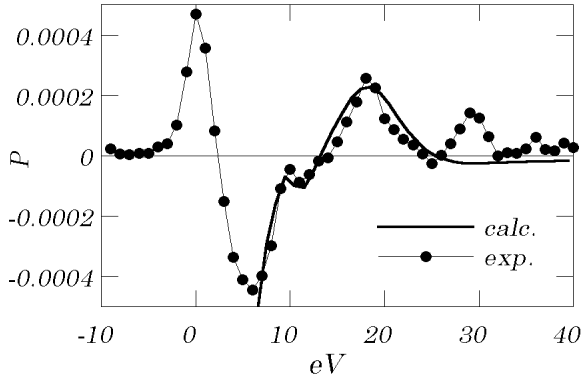

Figure 4
The calculated Fe K-edge XMCD spectrum $P = (T^\infty(1,1) - T^\infty(-1,-1))/(T^\infty(1,1) + T^\infty(-1,-1))$ by use of the full multiple scattering approach for a cluster with 59 iron atoms in bcc Fe. Experimental result is also shown for comparison (Mizumaki, 1996). The energy zero is set to be at the first inflection point in the absorption spectrum.

4. Conclusion

K-edge XMCD theory is described on the basis of semi-relativistic theory where spin-flip term is treated as weak perturbation. This severely restricts the application to light elements such as the first row transition metals. For many systems, angular dependence of K-edge XMCD is dominated by $\cos\beta$ term in eq. (12). However further study should be necessary to use $\cos\beta$ term in the analyses of XMCD spectra.

References

Ankudinov, A. L. & Rehr, J. J. (1995). *Phys. Rev. B* **52**, 10214–10220.
Brouder, Ch., Alouani, M. & Bennemann, K. H. (1996). *Phys. Rev. B* **54**,7334–7349.
Carra, P. & Altarrelli, M., (1990). *Phys. Rev. Lett.* **64**, 1286–1288.
Fujikawa, T. (1993). *J. Phys. Soc. Jpn.* **62**, 2155–2165.
Igarashi J., Hirai K., (1994). *Phys. Rev. B* **50**, 17820–17829.
Mizumaki, M. (1996). *Doctor thesis (The University of Tokyo).*
Schütz, G. & Ahlers, D. (1997). *J. Phys. IV FRANCE* **7**, C2-59 – 65.
Thole, B. T., Paoro Carra, Sette, F. & van der Laan, G., (1991). *Phys. Rev. Lett.* **68**, 1943–1946.
van der Laan, G., (1998). *Phys. Rev. B* **57**, 5250–5258.